Applied Surface Science 276 (2013) 832–837

Contents lists available at SciVerse ScienceDirect

Applied Surface Science

journal homepage: www.elsevier.com/locate/apsusc

# Hexagonally-arranged-nanoporous and continuous NiO films with varying electrical conductivity

A. Gutiérrez[a,*], G. Domínguez-Cañizares[a], J.A. Jiménez[b], I. Preda[c], D. Díaz-Fernández[a], F. Jiménez-Villacorta[d], G.R. Castro[c,e], J. Chaboy[f], L. Soriano[a]

[a] Departamento de Física Aplicada and Instituto de Ciencia de Materiales Nicolás Cabrera, Universidad Autónoma de Madrid, Cantoblanco, E-28049 Madrid, Spain
[b] Centro Nacional de Investigaciones Metalúrgicas, CSIC, Avda Gregorio del Amo 8, E-28040 Madrid, Spain
[c] European Synchrotron Radiation Facility, BP 220, F-38043 Grenoble Cedex 9, France
[d] Department of Chemical Engineering, Northeastern University, 360 Huntington Ave., Boston, MA 02115, USA
[e] Instituto de Ciencia de Materiales de Madrid, CSIC, Sor Juana Inés de la Cruz, 3, E-28049 Madrid, Spain
[f] Instituto de Ciencia de Materiales de Aragón, CSIC, and Departamento de Física de la Materia Condensada, Universidad de Zaragoza, E-50009 Zaragoza, Spain

ARTICLE INFO

*Article history:*
Received 23 November 2012
Received in revised form 25 February 2013
Accepted 2 April 2013
Available online 8 April 2013

*Keywords:*
Nickel oxide
Thin films
Nanostructured materials
Electrical conductivity
EXAFS
X-ray diffraction

ABSTRACT

Nickel oxide (NiO) thin films have been prepared by magnetron sputtering, with different $Ar/O_2$ ratios in the plasma, on several substrates, including hexagonally arranged nanoporous anodic alumina membranes (AAM). The obtained films exhibit columnar growth, which makes it possible to preserve the hexagonal order of the AAM substrates in the NiO thin films. X ray diffraction patterns show a polycrystalline structure with a crystallographic texture that depends on the plasma composition. Additionally, the NiO lattice parameter increases with the oxygen content of the plasma. The presence of oxygen during deposition is responsible for these structural changes, as well as for an oxygen enrichment in the NiO films, which leads to changes in their electrical properties. The electrical resistivity of the films decreases with the oxygen content of the plasma, which suggests p-type conductivity due to oxygen enrichment in the NiO lattice. Indeed, an analysis of the EXAFS oscillations at the Ni–K edge confirms the lattice expansion and a decrease of the Ni–Ni coordination number when the oxygen content of the plasma increases, which points towards an increasing presence of Ni vacancies for larger values of the $O_2/Ar$ ratio.


## 1. Introduction

Nanostructured oxide materials are currently the subject of intensive research due to their outstanding properties that make them attractive not only for fundamental studies, but also for a wide range of applications [1–3]. Among the transition metal oxides, nickel oxide can be found in several technological applications, such as electrochromic display devices, gas sensors, biosensors, solar cells, catalysis, electrochemical capacitors, or electrodes in lithium-ion batteries [4–12]. In many of these applications, such as in catalysis or gas, sensing, the interaction with the surrounding environment plays a very important role. The use of nanostructured materials increases the effective surface, and, consequently, enhances the yield of the surface reactions of interest.

Nickel oxide can be obtained by a variety of methods, both chemical [13–15] and physical [16–18]. Among the physical methods, reactive sputtering has been most widely used, giving high deposition rates, uniformity over large areas of the substrates and good control of the composition and structure of the deposited films. The final properties of the grown material depend on the main deposition parameters, such as substrate temperature, oxygen partial pressure, sputtering power, or distance between target and substrate.

According to the three zone model of Thornton [19] the final microstructure of sputter deposited coatings basically depends on the substrate temperature and the gas pressure. For low temperatures (compared to the adsorbate melting temperature) and high pressures (of the order of 10 mTorr), the resulting microstructure is very porous, formed by columns of material separated by voids. This is due to a low diffusion rate and to shadowing of the deposited material. This effect increases for oblique deposition angles. Since one of our objectives is to obtain nanoporous coatings at the nanoscale we have used low temperature, high pressure, and a certain deposition angle in our sputtering system to obtain NiO nanostructured coatings. We have used as substrates glass, silicon, and, to enhance the nanoporous growth of the films, anodic alumina

* Corresponding author. Tel.: +34 914 973 520.
*E-mail address:* a.gutierrez@uam.es (A. Gutiérrez).

0169-4332/$ – see front matter © 2013 Elsevier B.V. All rights reserved.
http://dx.doi.org/10.1016/j.apsusc.2013.04.007

nanoporous membranes. The obtained coatings were characterized by scanning electron microscopy (SEM) and X-ray diffraction (XRD). Electrical measurements were carried out to determine their electrical resistivity. A detailed analysis of EXAFS measurements taken at the Ni–K edge allowed us to correlate the measured electrical conductivity with the presence of Ni vacancies.

## 2. Materials and methods

NiO nanostructured coatings were grown by RF magnetron sputtering of a NiO target (AJA International, 99.95% purity). Different substrates were used in order to study the effects of the substrate surface morphology on the final properties of the NiO films. Glass microscope slides and single-crystal silicon wafers (p-type with (1 0 0) orientation) were used as planar substrates. Commercial (Synkera Technologies) anodic alumina membranes (AAM) grown on aluminum were used as nanostructured substrates. The pore diameter of the AAM was ~35 nm, and the distance between pores was ~100 nm, which gives a porosity of approximately 11%. The thickness of the AAM was 500 nm. Except for the AAM, all substrates were ultrasonically cleaned by immersing them subsequently in acetone and methanol. For a given sputtering condition, NiO was deposited simultaneously on all substrates, which guarantees that all samples were grown on different substrates under identical conditions.

NiO coatings were deposited at room temperature by RF magnetron sputtering in a high vacuum chamber with a base pressure $< 10^{-7}$ mbar. The pressure used for plasma ignition was $1.5 \times 10^{-2}$ mbar, and was maintained at this value during the whole growth process. The deposition time was 1 h. The plasma was composed of a mixture of oxygen and argon, with an oxygen content ranging from 0% to 70%. The substrates were rotated during deposition at about 10 rpm in order to obtain a more uniform film. The angle of the sputtering cathode with respect to the normal to the substrates surface was 23° (off-axis), and the distance between target and substrate was 8 cm. Before starting deposition a pre-sputtering of 5 min was performed in order to clean the target surface. The magnetron power was set to 100 W. Although no heating of the substrates was applied, a temperature increase of about 50 °C, induced by the plasma, was observed at the surface of the substrates at the end of the deposition, as was monitored by an IR external pyrometer operating through a sapphire window.

X-ray diffraction (XRD) measurements were carried out with a Panalytical Xpert PRO diffractometer in grazing incidence condition. In the setup used, an X-ray tube providing Cu K-alpha radiation with the corresponding optical setup provides a parallel and monochromatic X-ray beam. XRD data were collected with a beam incidence angle of 1° and $2\theta$ scan between 30 and 70° with a step size of 0.03° and a counting time of 5 s/step. In the Rietveld refinement, instrument functions were empirically parameterised from the profile shape analysis of a corundum sample measured under grazing incidence at the same conditions. The morphology of the deposited NiO films was observed by scanning electron microscopy (SEM), using a Philips XL30 S-FEG microscope equipped with a field-emission cathode, at an accelerating voltage of 20 kV. The electrical resistivity of the films was measured at room temperature by the Van der Pauw method using an Ecopia HMS-5000 system.

XAS spectra were measured above the Ni–K edge ($E \approx 8.3$ keV) at the SpLine BM25 experimental station of the European Synchrotron Radiation Facility (ESRF) in Grenoble, France. Measurements were carried out at room temperature in fluorescence mode, using a multi-element solid-state multichannel detector. The XAS spectra were processed according to standard procedures [20] and the EXAFS signals were analyzed by using the VIPER program [21]. Every measurements and fittings were systematically performed on samples deposited on AAM and Si substrates, with no significant difference.

## 3. Results and discussion

Fig. 1 shows SEM images of NiO coatings grown with 50% oxygen content in the plasma on nanoporous AAM (images 1a and 1b) and on flat Si substrates (images 1c and 1d). As it can be clearly seen in Fig. 1a, the hexagonal structure of the AAM substrate is kept in the NiO film after deposition, which results in the formation of a hexagonally arranged NiO nanoporous film. This behavior was observed for all samples grown on AAM substrates with different oxygen content in the plasma, from 0% to 70%. Fig. 1b shows a cross section of the same membrane as the one shown in Fig. 1a. The columns that build up the hexagonal nanoporous structure are clearly seen. The top bright end of the columns corresponds to the NiO coating, whereas the darker region below corresponds to the AAM substrate. As the image shows, NiO grows only on top of the alumina walls, without blocking or filling the pores. The thickness of the NiO film according to the SEM image is approximately 100 nm. Fig. 1c and d shows a NiO coating grown under the same conditions on a flat surface, in this case on a Si single crystal. The top view shows a very fine, disordered structure, with grain sizes of about 20 nm. The cross section shown in Fig. 1d clearly reveals that each of these grains is in fact the top side of a columnar grain that covers most of the coating thickness. This columnar type of growth can help to explain why the pores of the AAM substrate are kept after NiO deposition, as is shown in Fig. 1a and b: NiO deposits on top of the AAM walls, and the lack of lateral growth keeps the columnar growth in the vertical direction.

Fig. 2 shows X-ray diffraction patterns of NiO samples grown on Si with different plasma compositions. Samples grown on AAM substrates were also measured, but the overlap of NiO peaks with the signal coming from the AAM aluminum support prevented a satisfactory analysis. Consequently, the following discussion on X-ray diffraction concerns only NiO films deposited on flat substrates. The oxygen content of the plasma is shown at the right of each curve. The bottom curve corresponds to the sample grown with pure argon plasma. It shows the typical features of cubic NiO, with the (1 1 1) peak at 36.8°, the (2 0 0) peak at 42.9°, and the (2 2 0) peak at 62.3°.

Compared with the intensity of the standard $2\theta$ peaks reported on the ICDD card for bunsenite [22], the (2 0 0) peak has a higher relative intensity than expected, which indicates that the film growth follows preferentially this orientation. Similar behavior has already been reported for other nanostructured NiO films [13]. The features observed in the range between 53° and 57° come from the silicon substrate and are observed in all samples. The addition of oxygen to the sputtering plasma has remarkable effects on the structure of the grown films. First, a broadening of the peaks and a decrease of their intensity is clearly observed, the latter evidenced by a decrease in the signal to noise ratio. These changes can be associated to more disorder, smaller grain size, and even lattice microstrains. The topmost curve, which corresponds to the sample grown with maximum oxygen content, seems to revert this trend, showing narrower and more intense peaks than other samples grown with a lower oxygen content. A second effect of the oxygen addition on the films growth is the change of preferential orientation. Already for 10% $O_2$, the prevalence of the (2 0 0) peak disappears, with an intensity ratio closer to standard polycrystalline NiO [22]. By increasing the oxygen content of the plasma, the (1 1 1) and (2 2 0) peaks gradually increase, while the (2 0 0) relative peak intensity decreases. The final situation, for 70% oxygen, shows a clear preferential orientation along the (1 1 1) direction. Although there are some works in

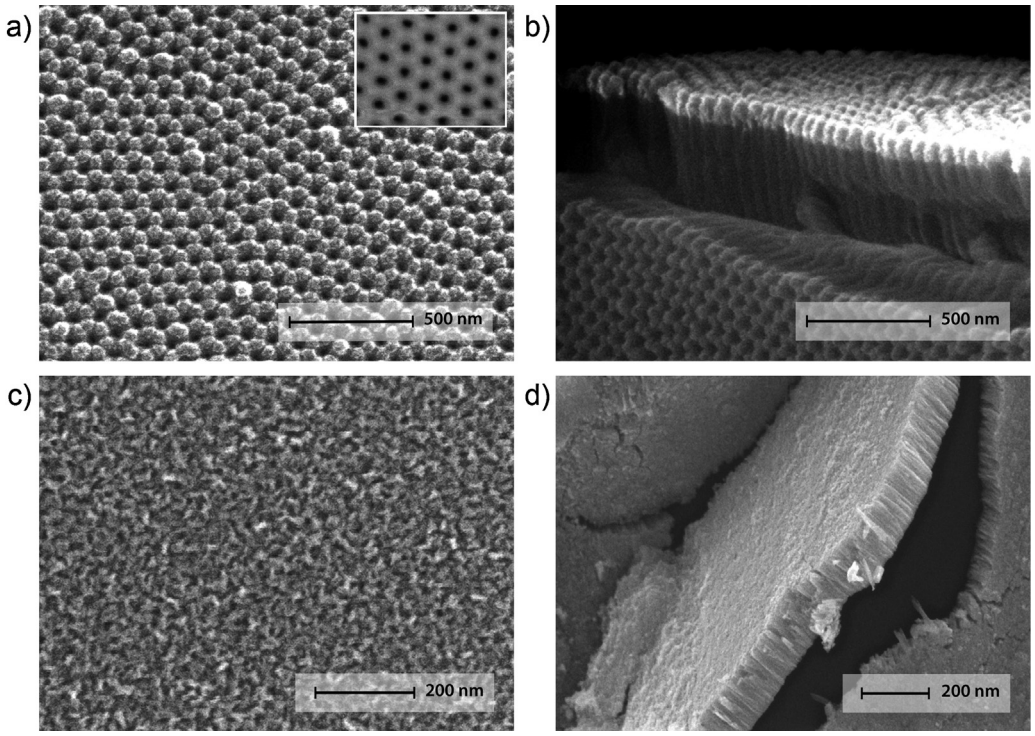


**Fig. 1.** High resolution SEM images of NiO coatings deposited on an AAM substrate – (a) and (b) – and on a Si single crystal – (c) and (d). Images (a) and (c) show top views and images (b) and (d) show cross sections of the films. The inset in image (a) shows a top view of the nanoporous alumina substrate before NiO deposition. The ratio of $Ar/O_2$ in the plasma during sputtering of this sample was 1/1.

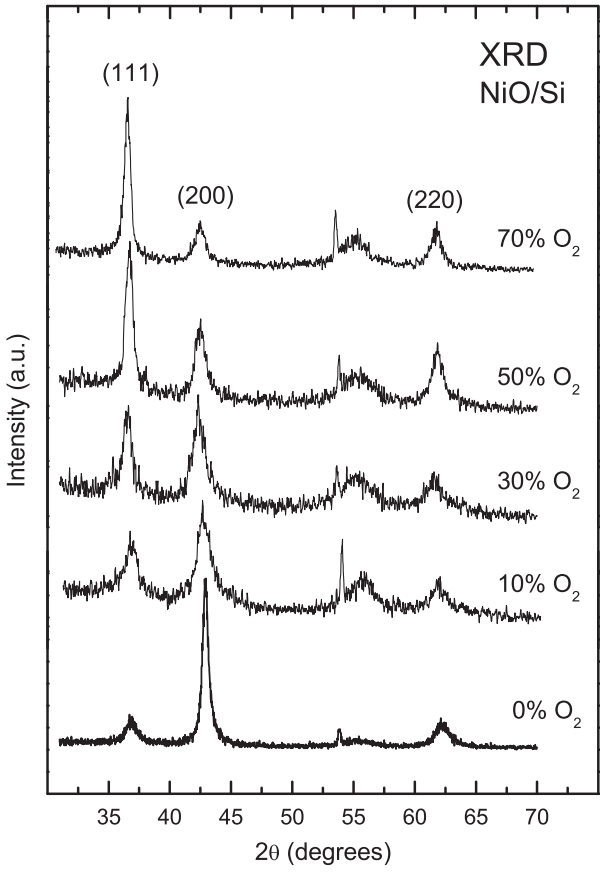


**Fig. 2.** X-ray diffraction patterns of NiO samples grown on Si with different oxygen content in the sputtering plasma. Measurements were taken in grazing incidence condition with monochromatic X-rays from a Co tube.

the literature reporting the evolution of the crystallographic texture with the oxygen content, there is not a clear uniformity in the trends [5,23–25]. In any case, it is clear that, while the columnar growth shown in Fig. 1 is kept for all samples, the crystal orientation of the columns seems to depend very strongly on the oxygen content of the plasma. The prevalence of the (1 1 1) peak for a higher oxygen ratio in the plasma is probably related to free energy considerations of the NiO growth in an oxygen-rich atmosphere, as has been proposed in a previous work [23].

Additionally to the mentioned changes in the diffraction patterns, a slight shift of the peaks towards lower angles can also be observed, which suggests an increase of the lattice parameter. In order to quantify this effect, the curves were fitted using a standard Rietveld refinement procedure. The results are shown in Fig. 3, where the lattice parameter of standard polycrystalline NiO ($a$ = 4.177 Å [22]) is also shown for comparison. The value obtained for the sample grown under pure Ar atmosphere is slightly larger than that of the NiO reference, suggesting a small lattice expansion for this sample. The expansion increases with the oxygen content of the plasma, although this increase slows down at higher oxygen contents. A similar increase of the lattice parameter with the oxygen content of the plasma has already been observed in a previous work [25]. This lattice expansion, together with the lattice disorder and microstrains observed in Fig. 2, might be originated by excess oxygen in the NiO lattice. The presence of oxygen ions in the plasma and their interaction with the NiO target would produce oxygen-enriched NiO particles that would be projected against the substrates. Such oxygen enrichment would produce Ni vacancies in the NiO lattice, and, if this is the case, the Ni–Ni mean coordination number should decrease. EXAFS is an experimental technique that can give both interatomic distances and coordination numbers of the first neighbor layers around an emitter atom. Consequently, this technique can help to confirm the previous hypothesis.

The comparison of the Ni K-edge $k^2$–weighted EXAFS signals and their Fourier transforms (FTs) are shown in Fig. 4. The EXAFS signals

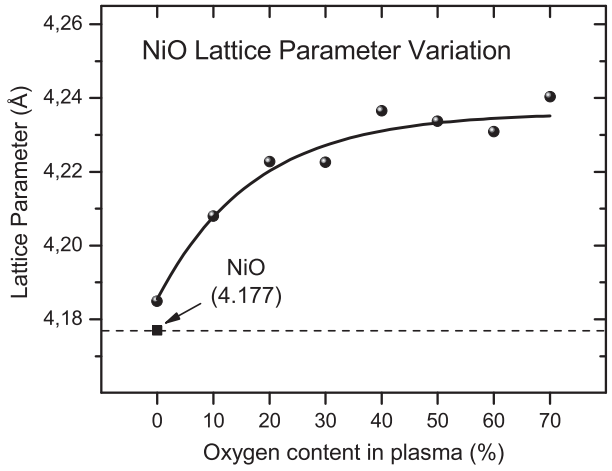


**Fig. 3.** Evolution of the lattice parameter of NiO coatings deposited on Si substrates with the oxygen content in the sputtering plasma. Lattice parameter values were obtained by Rietveld refinement of the original data.

have been obtained after removing the background by a cubic spline polynomial fitting and by normalizing the magnitude of the oscillations to the edge jump. The corresponding pseudoradial distribution function around the absorbing atom has been obtained by performing the Fourier transform using a Hanning window in the range $2.3 \leq k \leq 10.3$ Å$^{-1}$. For this comparative study, the Fourier transform of the EXAFS signals was performed within the same $k$-range. Fig. 4a shows the EXAFS signal of samples grown with 0% $O_2$ and with 70% $O_2$, respectively. The frequency of the oscillations is very similar in both cases, but a larger amplitude damping is clearly observed for the 70% sample at high $k$-values. This damping occurs gradually along the whole series, increasing from 0% to 70%, so the data shown in Fig. 4a correspond to the sample with the highest amplitude (0% $O_2$) and that with the lowest amplitude (70% $O_2$). Such a decrease in the amplitude of the EXAFS oscillations can be caused by either a decrease of the coordination number or an increase of the structural disorder. In order to distinguish which effect is responsible for the amplitude damping, a precise analysis of the EXAFS data is required.

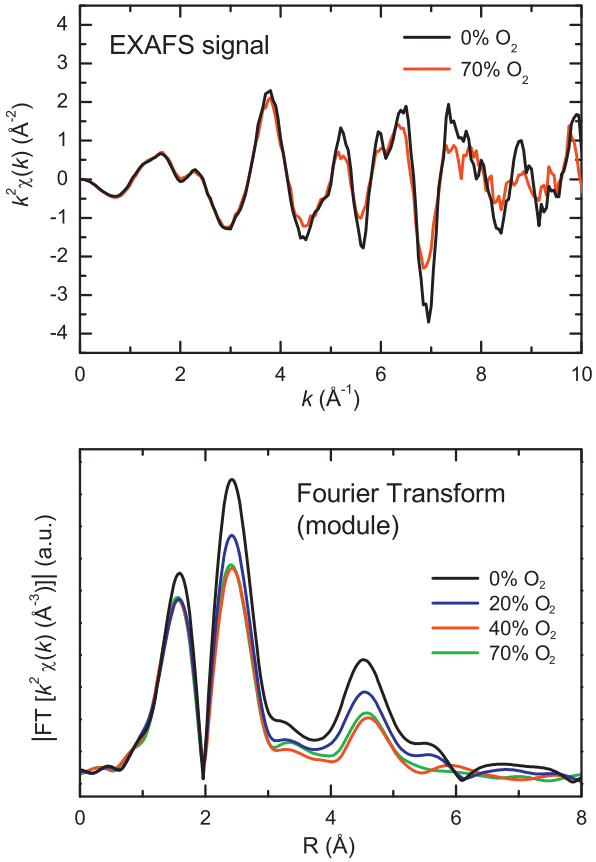


**Fig. 4.** (a) EXAFS signal obtained from the X-ray absorption spectra of samples grown with 0% $O_2$ and with 70% $O_2$ in the plasma, respectively. Data have been scaled by $k^2$ to enhance the EXAFS oscillations at higher $k$ values; (b) module of the Fourier Transform (FT) of the EXAFS signal obtained for samples grown with 0%, 20%, 40%, and 70% $O_2$ in the plasma.

Fig. 4b shows the module of the Fourier transform (FT) of the EXAFS signal obtained for samples grown with 0%, 20%, 40% and 70% oxygen in the plasma. Phase corrections have not been included, so the position of the peaks differs by ~0.5 Å from their correct values. The first peak, at an approximate position of 1.5 Å, corresponds to the Ni–O first-neighbor distance, and the second peak, located at ~2.5 Å, to the Ni–Ni second-neighbor distance. The broad region above 3 Å corresponds to the contribution from multiple scattering events and from outer shells, made up of several Ni—Ni and Ni—O bonds, although the contribution of Ni—Ni bonds dominates [26]. Similarly to the amplitude of the EXAFS oscillations, the height of the peaks in the EXAFS FT curves is related to the structural disorder and the coordination number. In the cubic NiO lattice, each nickel atom is surrounded by a first-neighbor shell with 6 oxygen atoms, and by a second-neighbor shell with 12 nickel atoms. This explains the larger height of the Ni–Ni peak as compared to that of the Ni–O one observed in all curves shown in Fig. 4b. The intensity of the Ni–O peak clearly decreases down to a certain level upon oxygen addition to the plasma. On the other hand, the decrease of the Ni–Ni peak and that of the outer shells features is more gradual, with an intermediate level for the 20% sample, and a lower level for the 40% and 70% samples. Note that the Ni–Ni peak relative intensity of the 70% sample with respect to the 0% sample is much lower than that of the Ni–O peak for the same samples.

Similar EXAFS results have been previously reported on different NiO nanostructured systems [26,27]. In these works, a damping of the EXAFS signal and a consequent decrease of the FT peaks has also been observed, and explained in terms of lattice relaxation at the grain boundaries of nanocrystalline samples. Such relaxation produces an increase of the structural disorder, a decrease of the coordination number, and a slight expansion of the crystal lattice. In our case, the nanostructured morphology shown in Fig. 1, together with the expected oxygen enrichment induced by the presence of oxygen in the plasma during growth, should lead to similar results. With this in mind, we have performed a quantitative EXAFS analysis by using the phase and amplitude transferability method [28]. The backscattering amplitude, phase, and photoelectron mean free path factor were obtained from the experimental EXAFS spectra of the appropriate reference compound, in our case the sample grown with 0% oxygen in the plasma. In this way the Fourier filtered EXAFS contribution of the first two coordination shells was obtained by back-transforming the FTs in the $1.0 \leq r \leq 3.2$ range using a Hanning window. Least 'squares fitting of the extracted signals was performed by using VIPER [21]. The fitting procedure was systematically performed for samples deposited on AAM and Si substrates, with no significant difference. The results are shown in Table 1. The analysis of the bond lengths reveals a lattice expansion of about 0.5% when going from 0% to 70% oxygen in the plasma, which is consistent with the lattice expansion found by XRD. The difference between both values is probably originated by relaxation of the atomic positions around the Ni vacancies, as it is proposed in reference [29]. The Debye–Waller factor increases with the oxygen content of the plasma. This parameter is related to the relative displacement of the atoms with respect to their mean positions, i.e., to the structural disorder, and is indicative of increasing

**Table 1**
Results of the fitting analysis of the EXAFS data obtained on NiO films grown with different oxygen content in the plasma for the first two shells: 1 (Ni–O) and 2 (Ni–Ni). The maximum uncertainty in the coordination number is of the order of 10%.

| SAMPLE % oxygen | Coordination number | | Neighbour Distance (Å) ± 0.003 | | Debye–Waller factor (Å2) ± 0.002 | |
|---|---|---|---|---|---|---|
| | N1 | N2 | R1 | R2 | S1 | S2 |
| 0 | 6 | 12 | 2.084 | 2.954 | 0.010 | 0.010 |
| 10 | 6 | 11.8 | 2.084 | 2.954 | 0.010 | 0.011 |
| 20 | 6 | 11.7 | 2.084 | 2.958 | 0.012 | 0.012 |
| 30 | 6 | 11.7 | 2.080 | 2.958 | 0.011 | 0.012 |
| 40 | 6 | 11.4 | 2.082 | 2.966 | 0.014 | 0.013 |
| 50 | 6 | 11.3 | 2.083 | 2.966 | 0.014 | 0.014 |
| 60 | 6 | 11 | 2.083 | 2.965 | 0.013 | 0.013 |
| 70 | 6 | 11 | 2.082 | 2.966 | 0.014 | 0.014 |

disorder/strain through increasing oxygen incorporation. Finally, the coordination number decreases with the oxygen content of the plasma. In the case of the Ni—Ni bond, this parameter could be set to 12 for the sample grown with 0% $O_2$, but it gradually decreased with the oxygen content. Best fits (see Table 1) indicate that the Ni–Ni coordination number gradually decreases down to ~11 for the sample grown with 70% $O_2$. Although the maximum uncertainty in the coordination number determination is of the order of 10%, these results point towards an increasing presence of Ni vacancies as the oxygen content of the plasma increases, in agreement with recent results reported by Anspoks et al. on nanosized NiO [29]

The presence of Ni vacancies, with the consequent oxygen enrichment, is expected to have some effect on the macroscopic properties of the deposited films, especially in their electrical properties [25,30–32]. In Fig. 5 we show the resistivity of the NiO films grown on a flat insulating substrate, in this case glass, and on the AAM nanoporous substrates. In both cases there is a clear decreasing trend with the oxygen content of the plasma. Resistivity values of samples grown on AAM substrates are higher than those of samples grown on flat substrates by approximately two orders of magnitude. This difference must be related to the presence of pores in the first case, which hinder the in-plane electronic movement, increasing the resistivity. In any case, for both substrates the effect of increasing the oxygen content of the plasma is to reduce the electrical resistivity. This trend has already been observed in previous works [16,30,31]. By comparing this figure with Fig. 3, one can observe a clear correlation between the measured resistivity and the lattice parameter. The larger the oxygen content of the plasma, the larger the lattice parameter, and the lower the electrical resistivity. Even sample grown with 0% oxygen, with a lattice parameter slightly higher than stoichiometric NiO shows a reduced resistivity value [32]. The observed changes in resistivity are correlated to the concentration of Ni vacancies, i.e., to the coordination number observed by EXAFS: the lower the Ni–Ni coordination number, the lower the resistivity. Interestingly, the EXAFS analysis shows a similar behavior for samples grown with 40% and 70% oxygen in the plasma, which agrees with the saturation-like trend observed in the lattice parameter variation and in the electrical resistivity measurements. NiO is very usually reported as a p-type semiconductor [16]. This electrical behavior is based on the conduction by holes. The observed oxygen enrichment in the NiO lattice, with the appearance of Ni vacancies, would create the necessary holes to produce p-type conduction. This oxygen enrichment would also produce a distortion of the NiO lattice, which would result in the lattice expansion observed in Fig. 3.

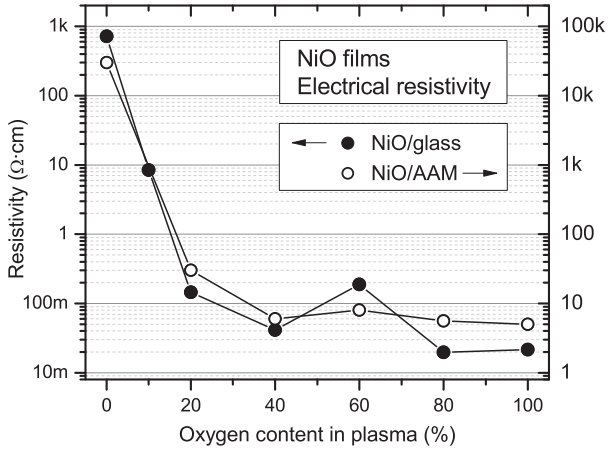


**Fig. 5.** Evolution of the electrical resistivity of NiO films grown on different substrates with the oxygen content in the sputtering plasma.

## 4. Conclusions

We have grown NiO thin films by magnetron sputtering with mixed $Ar/O_2$ plasma on several substrates. The films grow in columns, with crystallographic textures that depend on the oxygen content of the plasma, being the (2 0 0) direction the preferential one at lower oxygen content, and the (1 1 1) direction that at higher oxygen content. The films grown on alumina nanoporous membranes keep the porous structure of the substrates, which results in NiO hexagonally ordered nanoporous structures. An increase of the lattice parameter with the oxygen content of the plasma, together with a broadening of the diffraction peaks, was observed. The analysis of the diffraction curves reveals a lattice expansion of about 1% associated with the oxygen content of the plasma. On the other hand, EXAFS data show a decrease of the Ni–Ni coordination number when the oxygen content of the plasma increases, which can only be explained by an increasing presence of Ni-vacancies in the NiO lattice. Both the lattice expansion and the presence of Ni vacancies seem to be correlated with the electrical behavior of the samples. The electrical resistivity of the NiO films decreases with the oxygen content of the plasma, which is consistent with p-type conductivity originated by an oxygen enrichment in the NiO lattice.

## Acknowledgements

This work has been supported by the Spanish MICINN, under projects ENE2010-21198-C04-04, CSD2008-0023, and MAT2011-27573-C04-04. We acknowledge the European Synchrotron Radiation Facility (ESRF) and the SpLine CRG beamline staff for provision of synchrotron radiation and for assistance during X-ray absorption experiments.

## References

[1] A.S. Arico, P. Bruce, B. Scrosati, J.M. Tarascon, W. Van Schalkwijk, Natural Materials 4 (2005) 366–377.
[2] J.G. Lu, P. Chang, Z. Fan, Materials Science and Engineering R 52 (2006) 49–91.
[3] M. Fernández-García, A. Martínez-Arias, J. Hanson, J. Rodriguez, Chemical Reviews 104 (2004) 4063–4104.

[4] S. Yamada, T. Yoshioka, M. Miyashita, K. Urabe, M. Kitao, Journal of Applied Physics 63 (1988) 2116–2119.
[5] I. Hotovy, J. Huran, P. Siciliano, S. Capone, L. Spiess, V. Rehacek, Sensors and Actuators B: Chemical 78 (2001) 126–132.
[6] N.D. Hoa, S.A. El-Safty, Chemistry – A European Journal 17 (2011) 12896–12901.
[7] M. Tyagi, M. Gomar, V. Gupta, Analytica Chimica Acta 726 (2012) 93–101.
[8] K. Arora, M. Tomar, V. Gupta, Biosensors and Bioelectronics 30 (2011) 333–336.
[9] M.D. Irwin, B. Buchholz, A.W. Hains, R.P.H. Chang, T.J. Marks, Proceedings of the National Academy of Sciences of the United States of America 105 (2008) 2783–2787.
[10] T. Lai, C. Lee, K. Wu, Y. Shu, C. Wang, Applied Catalysis B: Environmental 68 (2006) 147–153.
[11] V. Srinivasan, J. Weidner, Journal of the Electrochemical Society 144 (1997) L210–L213.
[12] S.A. Needham, G.X. Wang, H.K. Liu, Journal of Power Sources 159 (2006) 254–257.
[13] A. Bachmann, A. Zolotaryov, O. Albrecht, S. Goetze, A. Berger, D. Hesse, D. Novikov, K. Nielsch, Chemical Vapor Deposition 17 (2011) 177.
[14] K. Liu, M. Anderson, Journal of the Electrochemical Society 143 (1996) 124–130.
[15] M. Feygenson, A. Kou, L.E. Kreno, A.L. Tiano, J.M. Patete, F. Zhang, M.S. Kim, V. Solovyov, S.S. Wong, M.C. Aronson, Physical Review B 81 (2010) 014420.
[16] H. Sato, T. Minami, S. Takata, T. Yamada, Thin Solid Films 236 (1993) 27–31.
[17] B. Sasi, K.G. Gopchandran, Nanotechnology 18 (2007) 115613.
[18] W.L. Jang, Y.M. Lu, W.S. Hwang, C.L. Dong, P.H. Hsieh, C.L. Chen, T.S. Chan, J.F. Lee, Epl-Europhysics Letters 96 (2011) 37009.
[19] J.A. Thornton, Journal of Vacuum Science and Technology A: Vacuum Surfaces and Films 4 (1986) 3059–3065.
[20] D.E. Sayers, B.A. Bunker, in: D.C. Koningsberger, R. Prins (Eds.), X-Ray Absorption: Principles, Applications, Techniques of EXAFS, SEXAFS, and XANES", Wiley, New York, 1988 (Chapter 6).
[21] (a) K.V. Klementiev, Nuclear Instruments and Methods A 448 (2000) 299–301; (b) K.V. Klementiev, Journal of Physics D: Applied Physics 34 (2001) 209–217.
[22] Powder Diffraction File PDF 00-047-1049 (International Center of Diffraction Data, ICDD).
[23] H.W. Ryu, G.P. Choi, W.S. Lee, J.S. Park, Journal of Materials Science 39 (2004) 4375–4377.
[24] A. Karpinski, A. Ferrec, M. Richard-Plouet, L. Cattin, M.A. Djouadi, L. Brohan, P.Y. Jouan, Thin Solid Films 520 (2012) 3609–3613.
[25] D. Soo Kim, H. Chul Lee, Journal of Applied Physics 112 (2012) 034504.
[26] A. Kuzmin, J. Purans, A. Rodionov, Journal of Physics: Condensed Matter 9 (1997) 6979–6993.
[27] A. Anspoks, A. Kuzmin, Journal of Non-Crystal Solids 357 (2011) 2604–2610.
[28] P.H. Citrin, P. Eisenberger, B.M. Kincaid, Physical Review Letters 36 (1976) 1346–1349.
[29] A. Anspoks, A. Kalinko, R. Kalendarev, A. Kuzmin, Physical Review B 86 (2012) 174114.
[30] Y.H. Kwon, S.H. Chun, J.-H. Han, H.K. Cho, Metals and Materials International 18 (2012) 1003–1007.
[31] O. Kohmoto, H. Nakagawa, F. Ono, A. Chayahara, Journal of Magnetism and Magnetic Materials 226 (2001) 1627–1628.
[32] D. Adler, J. Feinleib, Physical Review B 2 (1970) 3112–3134.